https://doi.org/10.1016/j.envpol.2020.114655

Health risk-oriented source apportionment of $PM_{2.5}$-associated trace metals

Jiawen Xie[1,2], Ling Jin[1,2], Jinli Cui[1,3], Xiaosan Luo[4], Jun Li[5], Gan Zhang[5], Xiangdong Li[,1,2]*

[1]Department of Civil and Environmental Engineering, The Hong Kong Polytechnic University, Hung Hom, Kowloon, Hong Kong

[2]The Hong Kong Polytechnic University Shenzhen Research Institute, Shenzhen 518057, China

[3]Key Laboratory for Water Quality and Conservation of the Pearl River Delta, Ministry of Education, School of Environmental Science and Engineering, Guangzhou University, Guangzhou 510006, China

[4]International Center for Ecology, Meteorology, and Environment, School of Applied Meteorology, Nanjing University of Information Science and Technology, Nanjing 210044, China

[5]State Key Laboratory of Organic Geochemistry, Guangzhou Institute of Geochemistry, Chinese Academy of Sciences, Guangzhou 510640, China

*Corresponding author

Email: cexdli@polyu.edu.hk; Tel.: +852 2766 6041; Fax: +852 2334 6389

Abstract

In health-oriented air pollution control, it is vital to rank the contributions of different emission sources to the health risks posed by hazardous components in airborne fine particulate matters ($PM_{2.5}$), such as trace metals. Towards this end, we investigated the $PM_{2.5}$-associated metals in two densely populated regions of China, the Yangtze River Delta (YRD) and Pearl River Delta (PRD) regions, across land-use gradients. Using the Positive Matrix Factorization (PMF) model, we performed an integrated source apportionment to quantify the contributions of the major source categories underlying metal-induced health risks with information on the bioaccessibility (using simulated lung fluid) and speciation (using synchrotron-based techniques) of metals. The results showed that the particulate trace metal profiles reflected the land-use gradient within each region, with the highest concentrations of anthropogenically enriched metals at the industrial sites in the study regions. The resulting carcinogenic risk that these elements posed was higher in the YRD than in the PRD. Chromium was the dominant contributor to the total excessive cancer risks posed by metals while manganese accounted for a large proportion of non-carcinogenic risks. An elevated contribution from industrial emissions was found in the YRD, while traffic emissions and non-traffic combustion (the burning of coal/waste/biomass) were the common dominant sources of cancer and non-cancer risks posed by metals in both regions. Moreover, the risk-oriented source apportionment of metals did not mirror the mass concentration-based one, suggesting the insufficiency of the latter to inform emission mitigation in favor of public health. While providing region-specific insights into the quantitative

contribution of major source categories to the health risks of $PM_{2.5}$-associated trace metals, our study highlighted the need to consider the health protection goal-based source apportionment and emission mitigation in supplement to the current mass concentration-based framework.

Key words

$PM_{2.5}$; trace metal; source apportionment; bioaccessibility; health risk; land-use gradient

Capsule

The study presents a quantitative attribution of major sources to the health risks posed by $PM_{2.5}$-associated metals with incorporation of bioaccessibility and speciation.

1. Introduction

Air pollution has become a global environmental issue. About 91% of the world's population is exposed to polluted air at levels exceeding the World Health Organization (WHO)'s guideline value on air quality, and suffer from various health risks (WHO, 2018). $PM_{2.5}$ (particulate matter with an aerodynamic diameter of 2.5 μm or less) is considered a major component of air pollutants, and the cause of up to 4.2 million premature deaths worldwide every year (WHO, 2018). Due to its small size, $PM_{2.5}$ can enter the respiratory tract and later penetrate the bronchi. The ultrafine portion is even capable of penetrating deep into the alveoli, which can have adverse effects on human

health. It has been observed in many epidemiological studies that hospital admissions related to respiratory and cardiovascular diseases escalate under short-term and long-term exposure to $PM_{2.5}$, indicating that $PM_{2.5}$ can have acute and chronic effects on health (Atkinson et al., 2014; Thurston et al., 2016).

The fact that $PM_{2.5}$ can be associated with a number of pollutants, including toxic trace metal(loid)s and organics (e.g., polycyclic aromatic hydrocarbons (PAHs)) due to its large specific surface areas, significantly increases its mutagenic and carcinogenic risks. The accumulated evidence indicates that transition metals in fine particles are closely associated with oxidative DNA damage despite their low mass in comparison with other components (Sørensen et al., 2005; Lu et al., 2008). With the objective of evaluating the causative toxicity of $PM_{2.5}$-associated metals, many studies have been conducted on the concentrations and spatial-temporal variations of different metals embedded in $PM_{2.5}$, which relied on either a long-term monitoring campaign or transitory sampling events (Kendall et al., 2011; Wang et al., 2015; Liu et al., 2017; Wang et al., 2018).

As trace elements that enter the human body via $PM_{2.5}$ may not all be available for biochemical reactions, simulated lung fluids have been utilized to extract bioaccessible metal fractions to deduce the *in vivo* bioavailability of those trace metals for assessments of their inhalational health risks. The neutral Gamble's solution and acidic artificial lysosomal fluid are the most widely used solutions in *in vitro* tests of the

bioaccessibility of metals in atmospheric particles (Cong et al., 2011; Zereini et al., 2012; Huang et al., 2016a; Huang et al., 2016b; Ming et al., 2017).

While the bioavailability of trace metals is important, the health impact posed by a metal is also related to its toxic potency, which is highly dependent upon its chemical form and valence state (Jan et al., 2015; Egorova et al., 2017). Arsenic is one of the notable examples of metals that show great disparities in toxicity between different forms. It was observed that inorganic As(V) was the predominant species, accounting for over 80% of the total arsenic content of the airborne particles in urban areas (Sánchez-Rodas et al., 2007; Yang et al., 2012; Huang et al., 2014). However, the use of the inhalation unit risk (IUR) and reference concentration (RfCi) of metals in their most toxic form or based on their general bulk is a common practice in risk assessments, regardless of their valence as given by the United States Environmental Protection Agency (USEPA). This often results in large discrepancies from the environmental realm, and causes certain biases when comparing the inhalation risks in different studied areas, subject to variations in metal speciation. Therefore, it is important to consider modifications to conventional risk assessment methods by incorporating information on metal speciation.

In addition, various sources of airborne particulates and their chemical components, such as coal combustion, vehicular exhaust, dust resuspension, and industrial emissions, were identified using a number of source apportionment methods, including isotope

analysis (Cong et al., 2011) and mathematical applications like the chemical mass balance model (CMB) and positive matrix factorization (PMF) model (Tan et al., 2014; Qi et al., 2016; Chang et al., 2017). This information provided important references for the establishment of pollution control strategies. However, a limited integrated analysis has linked the source profiles of toxic components like trace metals with downstream health risk assessments to differentiate the contributions of various sources of emissions and the consequent health risks. Under the current assessment framework there are even fewer cases in which the chemical forms of metals and their bioaccessible fractions are taken into consideration. Doing so would make it possible to focus on the targeted sources of pollution, with significant health impacts. For example, a recent investigation based on bioavailable metals revealed that coal combustion and traffic emissions in Beijing in the wintertime are primarily responsible for the inhalational health risks in that city posed by airborne metals (Huang et al., 2018). Although the study was conducted over a short period, it placed a noteworthy focus on two critical sources in the health-oriented control of $PM_{2.5}$ pollution.

Considering that in recent decades, China has become one of the hotspots of severe $PM_{2.5}$ pollution, for this study we selected two of the most densely populated regions, namely, the Pearl River Delta (PRD) in the south and the Yangtze River Delta (YRD) region in the east, to conduct simultaneous $PM_{2.5}$ sampling over a period of a year across an urban-suburban-rural gradient. The PMF receptor model was used to resolve the question of the major sources of $PM_{2.5}$ components in those areas, with a focus on

trace metals. The carcinogenic and non-carcinogenic health risks were calculated using metal concentrations adjusted by bioaccessibility and speciation before being apportioned to different categories of emission sources. Our comprehensive study of the specific $PM_{2.5}$-associated health risks of two key regions in China with reference to their emission sources represents a significant contribution to the formulation of risk mitigation and pollution control strategies to improve regional air quality.

2 Materials and Methods

2.1 Sampling strategy and site description

Our $PM_{2.5}$ sampling campaign was conducted simultaneously in the YRD and PRD regions from March 2016 to February 2017. In each region, three sampling sites along land use gradients were selected: for the YRD, these were Pukou (PK, representing a suburban-industrial area), Xuanwu (XW, representing an urban area), and Lishui (LS, representing a rural area) of Nanjing; while for the PRD, these were Tianhe (TH, representing an urban area) and Conghua (CH, representing a suburban area) of Guangzhou, and Heshan (HS, representing a semirural-industrial area) of Jiangmen. For further details on the sampling sites, refer to the supplemental material (Figure S1; Tables S1 and S2). 24-hour $PM_{2.5}$ samples were collected weekly with high-volume samplers (TH-1000C II, Wuhan Tianhong Instruments Co., Ltd., China) at a flow rate of around 1 m^3/min, with the exception of LS, where samples were collected on a monthly basis. A summary of the total size of the samples for each site over the sampling period is given in Table S3. Tissuquartz filters of 8 × 10 inch (PALL, USA)

pre-baked at 500℃ for 5 h were used, weighed before and after sampling with a sensitivity of ± 0.0001 g. Before weighing, filters were equilibrated in a desiccator at 25℃ and at 40%-50% relative humidity for at least 24 h.

2.2 Chemical Analysis

$PM_{2.5}$ samples were subjected to multiple chemical analyses, including organic carbon (OC), elemental carbon (EC), water-soluble ions (WSI), total metal(loid)s, and bioaccessible metal(loid)s. OC and EC concentrations were analyzed using a Thermal/Optical Carbon Analyzer (Model 2001, Desert Research Institute) and calculated based on the results of the thermal optical reflectance (TOR) protocol. Major WSI (Na^+, K^+, NH_4^+, Cl^-, NO_3^-, and SO_4^{2-}) were extracted using Milli-Q water and analyzed by ion chromatography (Dionex). Total metal(loid)s and bioaccessible metal(loid)s extracted by Gamble's solution (one type of simulated lung fluid) (Marques et al., 2011) were analyzed via inductively coupled plasma-mass spectrometry (Agilent model 7700) after acid digestion. Further details of the pretreatment procedure and QA/QC for the metal(loid) analysis and the composition of Gamble's solution are presented in the supplemental material (Section S1; Table S4).

2.3 Source apportionment

The enrichment factors (EF) of metal(loid)s in $PM_{2.5}$ were calculated using Fe as the reference element, with comparisons to the geochemical background values of metal(loid)s in soils in Guangzhou and Jiangmen in the PRD region (Guangdong

175 Geological Survey, 2010) and in Nanjing in the YRD region (Liao et al., 2011). Then,
176 the PMF Model from USEPA (PMF 5.0) was applied to explore the more specific
177 sources of $PM_{2.5}$ (Norris et al., 2014) in the areas with intense human activities,
178 including two urban sites (TH, XW) and another two sites under industrial impact (HS,
179 PK), using the concentrations of $PM_{2.5}$ and its major chemical components. The
180 pretreatment process of the input data and the diagnosis of the output results are
181 described in the supplemental material (Section S2). To assess the uncertainty of the
182 modelled results, bootstrap run was applied for 100 times after the base run to estimate
183 the errors, which was used for the calculation of 95% confidence interval (CI).
184
185 *2.4 Analysis of arsenic speciation by X-ray absorption near edge structures (XANES)*
186 To explore the molecular speciation of arsenic in airborne fine particles, the As K-edge
187 (11,867 eV) XANES spectra of four selected $PM_{2.5}$ filter samples (*i.e.*, 3 from HS in
188 the PRD and 1 from PK in the YRD) with a high concentration of As were acquired in
189 fluorescence mode on beamline 01C1 at the National Synchrotron Radiation Research
190 Center (NSRRC), Taiwan, coupled with reference standards, such as $NaAsO_2$ and
191 Na_2HAsO_4. For the XANES analysis, $PM_{2.5}$ filter samples were directly used without
192 pretreatment, while standard compounds were ground into powder. Multiple scans for
193 each sample were merged and processed using Athena software (Ravel et al., 2005)
194 according to methods specified in previous studies (Cui et al., 2013; Cui et al., 2018)
195 before downstream linear combination fitting (LCF) was conducted, where all weights
196 were constrained to between 0 and 1 with a final sum of 1.

197

198 *2.5 Health risk assessment*

199 To determine the chronic inhalation risks caused by the airborne trace metals of interest,
200 a health risk assessment following guidelines from the USEPA was conducted based
201 on the bioaccessible concentrations for adults of metals detected in the sampling sites.
202 In light of the significant disparities in toxicity between different speciation of arsenic,
203 a slightly modified risk assessment was conducted. The distribution of each speciation
204 as determined by the XANES analysis was incorporated into the calculation of the
205 carcinogenic and non-carcinogenic risks it exerted.

206

207 Subsequent to the source apportionment results, the contribution of individual sources
208 to the carcinogenic risks (Con_{CR}) and to the non-carcinogenic risks (Con_{HQ}) of
209 metal(loid)s via inhalation were calculated using Equations 1 and 2, respectively.
210 Detailed algorithms pertaining to the health risk-based source apportionment
211 incorporating arsenic speciation can be found in Sections S3 and S4 of the supplemental
212 material.

213 $$Con_{CR_{s,l}} = \frac{CR_{s,l}}{\sum_s CR_{s,l}} \quad \text{(Eq 1)}$$

214 $$Con_{HQ_{s,l}} = \frac{HQ_{s,l}}{\sum_s HQ_{s,l}} \quad \text{(Eq 2)}$$

215 Where *s* represents an individual source category and *l* represents an individual
216 sampling location. $CR_{i,l}$ and $HQ_{i,l}$ are the carcinogenic risk and non-carcinogenic risk
217 induced by each metal (*i*) in a certain sampling location (*l*).

218

2.6 Data analysis

The data were processed using Excel, SPSS Statistics 21, and GraphPad Prism 7. The test of normality was conducted using QQ-plot and Shapiro-Wilk ($p<0.05$) to evaluate the distribution of the data. In this study, non-parametric tests using Kruskal-Wallis one-way analysis of variance (ANOVA) were employed to compare the differences between the sampling groups in the distribution of the data.

3 Results and Discussion

3.1 Inter-regional differences and intra-regional similarities in the concentrations and chemical composition profiles of $PM_{2.5}$

As a whole, residents in both the PRD and YRD region were exposed to polluted air almost all year round (March 2016-February 2017) at excessive $PM_{2.5}$ concentrations in comparison to the WHO guideline value (25 μg m^{-3} for 24-h samples) (Figure S2). Most of the highly polluted days in which $PM_{2.5}$ concentrations were above the Grade II value of the Chinese National Ambient Air Quality Standard (NAAQS) (75 μg m^{-3} for 24-h samples) fell in spring and winter, indicating seasonal characteristics in PM pollution. Generally, the $PM_{2.5}$ concentrations seemed to share similar patterns of fluctuation within the same region, with the exception of occasional site-specific episodes of pollution, such as the relatively high $PM_{2.5}$ concentrations in the semirural-industrial site (HS) in the PRD in winter (Figure S2). In terms of annual average $PM_{2.5}$ concentration (Figure S3), the HS site (69.0 μg m^{-3}) in the PRD and the PK site (68.6 μg m^{-3}) in the YRD, both subject to industrial influence, suffered from the heaviest air

241 pollution in their respective region, with a significantly higher concentration of $PM_{2.5}$
242 than in the suburban (CH, 46.7 μg m^{-3}) and rural (LS, 47.9 μg m^{-3}) areas, with the urban
243 sites in the middle of the range (TH, 50.0 μg m^{-3}; XW, 61.1 μg m^{-3}). Such discrepancies
244 among different land use zones were likely to reveal the exacerbation of air pollution
245 as a result of anthropogenic activities. Zooming into the urban sites of these two regions,
246 $PM_{2.5}$ concentrations were 20% higher in the YRD than in the PRD in terms of annual
247 average values (t-test, $p<0.05$), suggesting that urban residents in the YRD region are
248 vulnerable to exposure to air pollution.
249
250 Echoing the variations in $PM_{2.5}$ concentrations, the inter-regional differences in
251 chemical composition profiles were more pronounced than the intra-regional ones
252 (Figure 1). There was a higher proportion of water-soluble ions relevant to secondary
253 inorganic aerosols (NO_3^-, SO_4^{2-} and NH_4^+) and a lower proportion of carbonaceous
254 materials (organic matters (OM) and EC) presumably from combustion activities to the
255 total identified components in the YRD than in the PRD. Such regional differentiations
256 were also observed previously in these two regions regardless of the land-use type of
257 the sampling locations (Table S8) (Du et al., 2017; Ming et al., 2017; Tao et al., 2017).
258 The inter-regional heterogeneity in the dominant mass contributors of $PM_{2.5}$ (OM/EC
259 and WSI) underlined the regional $PM_{2.5}$ pollution characteristics and the discrepancies
260 in the major source contributors to $PM_{2.5}$ between the two regions.
261
262 *3.2 Regional comparisons of the characteristics of $PM_{2.5}$-associated metals*

263 In the PRD region, the annual average concentrations of the highly enriched (EF>100)
264 and some of the moderately enriched (10<EF<100) elements, such as Zn, Pb, As, and
265 Cd, were significantly higher in the semi-rural HS site than in the suburban and urban
266 sites (p<0.05) (Figure 2A, Table S9). Nevertheless, the remaining trace metals, such as
267 Cu, Cr, Ni, V, Mn, and Co, exhibited the lowest concentrations in the suburban CH site
268 (p<0.01) but showed elevated concentrations in the semi-rural (HS) and urban (TH)
269 areas. The highest concentrations of Zn, Pb, As, and Cd (regarded as industrial tracers),
270 which were found in HS, could be explained by the spread of industries containing
271 electroplate factories and hardware and battery manufacturers in this sampling district.
272 When comparing the situation in the YRD with that in the PRD, noticeable differences
273 were detected. As an important tracer of anthropogenic sources, such as metal
274 manufacturing and wear abrasions in transport activities, Cu was prominently shown to
275 have the highest concentration in the PK site, while the concentrations of other highly
276 or moderately enriched elements (Cd, As, Pb, Zn, Cr, and Ni) as well as V were either
277 comparable or slightly higher in the suburban-industrial PK site than in the urban XW
278 site, but significantly lower in the rural LS area (p<0.01). The intra-regional differences
279 in anthropogenic metal profiles in both the PRD and YRD indicated the spatial
280 heterogeneity of potential sources of emissions and their contribution to local pollution.
281 Different from some studies conducted in other countries where the metal concentration
282 gradient faithfully follow the urban-suburban-rural gradient (Hueglin et al., 2005), the
283 highest concentration of many highly and moderately enriched elements as industrial
284 and urban signals were found in a semi-rural site in the PRD and a suburban site in the

YRD. Similar trends were also found in previous studies targeting other pollutants in the PRD region (Chan et al., 2006). This can be explained by mixed land use and/or the expansion of urbanization and industrialization to the outskirts of cities, including suburban and even rural areas in certain regions of China. Furthermore, as mentioned above, the featured elements were found to be different in the PRD and YRD. On the basis of inter-regional comparisons, in the PRD a high abundance of Ni was found, which is an indicator of heavy oil usage (ship emissions in the PRD), and Co in the polluted areas, especially As at the semirural-industrial site (Figure 2A), corresponding to their higher levels of enrichment in this region (Figure S4). By contrast, there was a significant accumulation of Cr, Pb, Cd, and Cu in terms of absolute concentrations in non-rural sites in the YRD. Such differences are likely to reflect regionally distinctive patterns of pollution determined by disparities in sources of emissions and their underlying structure, affecting the risks of exposure to airborne metals by residents in different regions.

Bioaccessibility varied greatly among the targeted elements (Figure S5), referring to the modulation of the fraction of their bulk concentrations that can be readily available to lung cells in the human body. In general, the targeted elements exhibited spatially consistent bioaccessibility, with the highest for As (>60%), intermediate for Cu, Ni, Cd, and Co (20%-60%), and low for Zn, Fe, Cr, and Pb (<20%). In turn, as mentioned earlier, the spatial trend of the bioaccessible concentrations of these elements followed that of their total concentrations (Figures 2B and S5, Table S10). In contrast, the

bioaccessibility of Mn and V differed regionally, with higher bioaccessibility (>60%) in the PRD and lower bioaccessibility (20%-60%) in the YRD region. The difference in their total concentrations between the two regions (higher in the YRD than in the PRD) was thus eliminated. Our results were in agreement with those of previous studies, where As and V were observed to have high accessibility and Pb to have the lowest accessibility in airborne particles of different sizes in Gamble's solution (Wiseman et al., 2014). It was speculated accordingly that a large portion of the As, V, and Mn in $PM_{2.5}$ in this study existed as soluble ions, while the other studied metals were probably in refractory or non-dissolved forms. As mentioned earlier, the bioaccessibility of a metal depends largely on its chemical form only if the properties of the metal are taken into consideration. For example, Pb and Zn tend to be rich in submicron particles primarily in the form of oxides (Labrada-Delgado et al., 2012), which are difficult to leach out. This may partially explain the lower bioaccessibility of these two metal elements.

The solubility of airborne metals is determined by multiple factors, including source-dependent characteristics (*e.g.*, the metal-aerosol bond, metal speciation), operationally defined conditions (*e.g.*, the selected extraction solution), and environmental parameters (*e.g.*, pH and temperature) (Smichowski et al., 2005). Spatially, the bioaccessibility of most of the metals was consistent between sites within the YRD or within the PRD, which was in agreement with the intra-regional $PM_{2.5}$ pollution patterns reflected by the consistent chemical profile across regional scales (Figure 1).

329

330 *3.3 Speciation-adjusted risk assessment of metals*

331 The inhalational health risks posed by $PM_{2.5}$-associated metal(loid)s were calculated in
332 all of the sampling sites based on the annual average of the bioaccessible concentrations
333 for each targeted element, with a focus on both the carcinogenic risks (CR) and non-
334 carcinogenic risks (NCR) for adults. Regarding the effect potency of different metals,
335 the benchmark from the USEPA, coupled with other standards, generally correlated
336 with our previous cell-based toxicity assays, with the exception of Cr and Cu (Figure
337 3A). It was found that the USEPA guidelines of some metals were based on their most
338 toxic form or on a bulk application in which considerations of metal speciation were
339 omitted, such As and Cr, which could result in a bias in the risk assessment. The linear
340 combination fitting of the XANES spectra (Figure 3B) revealed that the predominant
341 form of arsenic was the less toxic pentavalent arsenic, which on average accounted for
342 90% of the arsenic (As(III)+As(V)) content in the PRD and almost 100% in the YRD
343 region, which is comparable to previous observations made in the PRD (Huang et al.,
344 2014). After modifying the CR and NCR of arsenic based on the speciation information
345 mentioned above, it was shown that at all sites the accumulated carcinogenic risk
346 exceeded the safety limit of 10^{-6}, ranging from 6.8×10^{-6} (suburban CH) to 1.3×10^{-5}
347 (semirural-industrial HS) in the PRD, and from 1.9×10^{-5} (rural LS) to 2.7×10^{-5}
348 (suburban-industrial PK) in the YRD. This pointed out the higher exposure risk for
349 residents in the YRD region than for those in the PRD region ($p<0.05$). If the current
350 exposure scenarios are sustained, around 6 to 12 and 19 to 27 adults out of every one

million in the population of the PRD and YRD regions, respectively, are at risk of developing cancer due to a lifetime exposure to airborne metals (Figure 4A). Among the potentially carcinogenic elements under consideration, chromium alone posed a cancer risk exceeding the acceptable level (10^{-6}) in all the sampling locations (Figure S6), accounting for over 95% of the total carcinogenic risks in the YRD and 74-90% in the PRD where arsenic was the second largest contributor (Figure 4B). For non-carcinogenic risks that were lower than unity at all sites, manganese took the place of chromium as the predominant contributor, with a risk contribution ranging from 39% at the CH site to 51% at the LS site. The only exception was the HS site, where arsenic became the top contributor to non-carcinogenic risks (38%). In addition, it was noteworthy that the lower toxic potencies of Fe and Zn, while at high concentrations, resulted in negligible cancer risks compared to other elements (Figure S8A).

3.4 Contribution of emission sources to metal-induced health risks

In order to further link the emission sources to the consequent health risks, two urban sites (TH and XW), and the two sites with strong industrial impacts (HS and PK) were selected for source apportionment using the PMF model (Figure S7; Section S5). For better spatial comparisons, sources with analogous attributes were combined and finally condensed into a total of five sources: fugitive dust and sea salts, industrial emissions, traffic emissions (vehicular emissions and fuel oil combustion by trucks and ships), non-traffic combustion (coal combustion, biomass burning, and waste incineration), and the formation of secondary aerosols (SA; secondary sulfate, nitrate, and organic

matters). The three typical anthropogenic sources, namely traffic emissions, non-traffic combustion, and industrial emissions, contributed a similar share (~50%) of the $PM_{2.5}$ mass concentration in both the YRD and PRD regions. However, the contribution of these sources to the mass concentration of risk-inducing metals differed between the two regions (<50% for the YRD and >75% for the PRD) (Figure 4D; Figure S8B). The non-traffic combustion identified in TH and HS site was partially mixed with secondary sulfate, thus leading to an overestimated contribution to $PM_{2.5}$ mass from non-traffic combustion and an underestimation from secondary aerosols to some extent in these two sites. Nevertheless, there was a negligible influence on the source-resolved profile of trace metal mass and metal-induced risks, as the metal contribution from secondary sulfate could be relatively low. For both the carcinogenic and non-carcinogenic risks, the source-resolved contribution was regionally distinct between the YRD and PRD regions, and relatively consistent between sites of different land-use within each region (Figure 4C; Figure S8B), reiterating the regional patterns of pollution. In the PRD, the first three largest source contributors of carcinogenic risks were traffic emissions (52-57%), non-traffic combustion (32-36%), and industrial emissions (0-10%). In contrast, industrial contribution was predominant in the YRD region (33% in XW and 46% in PK), with traffic emissions (35%) and non-traffic combustion (31%) in urban areas; but ranked first among the source contributors of CR in suburban-industrial PK. With regard to the non-carcinogenic risk, the NCR source profile appeared to be similar to the source-resolved contribution of the mass concentrations of risk-posing metals (Figure 4C and 4D). Traffic emissions (39% in TH and 32% in HS) and non-traffic

395 combustion (23% in TH and 26% in HS) remained the predominant sources of non-
396 carcinogenic risk by metals at most of the sites in the PRD, the only exception being
397 urban TH, where fugitive dust and sea salts (34%) outcompeted non-traffic combustion.
398 In the YRD, the major source contributor to NCR was non-traffic combustion activities
399 (42% in XW and 51% in PK), followed by comparable contributions from traffic and
400 industrial emissions. The regional differences in source-resolved metal mass/risk
401 profile reflected the different industrial and energy structures. For example, coal
402 consumption was greater in the YRD than in the PRD (National Bureau of Statistics of
403 China, 2014), resulting in a greater share of non-traffic combustion activities in the
404 mass concentration and NCR of metals in the YRD region. Previous studies also
405 demonstrated that industrial coal combustion accounted for the considerable metal-
406 induced health risks in another industrial city (Foshan) of the PRD (Zhou et al., 2018),
407 and identified coal combustion and traffic emission as the most dominant sources of
408 health risks posed by metals during wintertime $PM_{2.5}$ episodes in Beijing (Huang et al.,
409 2018). More importantly, these studies also highlighted the significant discrepancies
410 between mass concentration-based and health risk-based source apportionment of
411 $PM_{2.5}$-associated metals. Such discrepancies were also observed with other toxic
412 components, such as PAHs in urban Nanjing (Zhuo et al., 2017). These findings
413 prompted us to rethink the current framework of mass concentration-based source
414 apportionment and emission reduction for $PM_{2.5}$ pollution. As dominant mass fractions
415 (e.g., NO_3^-, SO_4^{2-}) are not necessarily toxicologically relevant, there is an imminent

need for identification of key toxic components and associated sources to support health risk-based source apportionment and mitigation strategies (Li et al., 2019a).

3.5 Implications and limitations

Linking the potential sources of emissions with the resultant health outcomes is of great significance in producing valuable information for health-oriented pollution control. In this study, the bioaccessible concentration rather than the total concentration of metals in $PM_{2.5}$ covering a complete seasonal cycle was applied for a source-specific risk assessment. This is closer to the real situation of metal uptake in human lungs, and representative of long-term metal exposure scenarios. The comparative study conducted in two of the most populous regions of China, with sampling sites along a clear geographical transect in each region, can help to shed further light on inter- and intra-regional differences.

The USEPA standard guideline for arsenic risk assessments is based on its bulk concentration. Looking into the sources of data used by the USEPA to derive the IUR and RfCi of arsenic for the risk assessment (USEPA, 2007; OEHHA, 2014), it was found that the percentage of As(III) could be somewhat higher in the studies that are referred to than in the general urban areas, possibly resulting in an overestimation of the contribution of As to the total exposure risk. This motivated us to adjust the measured concentration of total As by its speciation in a quantitative manner, which resulted in a more realistic assessment of the health risks by reducing the bias of mere

use of total concentrations. However, as the low concentration of Cr, whose toxic potency varies between chemical forms, did not suffice for the XANES analysis of its speciation, we did not apply the speciation-based adjustment in the risk assessment of Cr, which may thus lead to an overestimated risk contribution from Cr in this study. This highlights the need for more robust predications of the bioavailability and characterization of toxic metal forms in $PM_{2.5}$ in the future. Other heavy metals like Fe and Cu have previously been identified as dominant drivers of metal-induced oxidative stress in human lung cells exposed to urban $PM_{2.5}$ (Jin et al., 2019). This contrasts with the finding in the present study that these elements contributed little to the health risks of $PM_{2.5}$-associated metals. This is understandable because of the inconsistencies in the relative toxic potencies of metals between the two systems of assessment, as well as because of the incorporation in this study of bioaccessibility in lieu of total concentrations. It is therefore imperative to develop robust predictive models to reconcile the data on *in vitro* toxicity and the safety limits derived from human epidemiological studies on inhalable metals. As metals only accounted for a small proportion of the toxicity of $PM_{2.5}$ mixtures (Jin et al., 2019), in the future other chemical components, such as parent and substituted PAHs (Taghvaee et al., 2018; Li et al., 2019b) and microbial components (*e.g.*, bacterial endotoxins) (Mahapatra et al., 2018), which also contribute to PM toxicities, need to be analyzed collectively for an integrated assessment of the risks of inhaling $PM_{2.5}$ (Jin et al., 2017). Admittedly, the current risk assessment still replied on a number of default exposure and population parameters, which can be refined to reflect local scenarios in the future.

Our current exercise on health risk-oriented source apportionment was based on the assumption of the equal bioaccessibility of a certain metal element for various source categories, which was found to deviate from the real circumstance. Thus, it is necessary to investigate the speciation profile of metals in different sources and apportion the health risks to emission sources according to a more realistic basis – source-specific metal bioavailability. Nevertheless, the outcome of this study has practical implications for targeted mitigation instead of mass concentrations in the alleviation of health risks.

4 Conclusion

This study presented a comparative picture of regional patterns of $PM_{2.5}$ pollution, variations in $PM_{2.5}$-associated metals, as well as other chemical components along a city land-use gradient in the YRD (east China) and the PRD (south China) regions. This study also highlights the importance of incorporating bioaccessibility and the speciation of metal elements into assessments of health risks, which formerly were biased by the use of total metal concentrations. Coupling source apportionment using the PMF model with a risk assessment, we revealed that anthropogenic sources (e.g., traffic, combustion, industry) contributed >90% of the metal-induced cancer risk in the PRD and >95% in the YRD region, which was distinguished from their less contribution to metal mass concentrations (<50% in the PRD and >75% in the YRD). The quantitative insights connected the dots between the major source categories and the resultant health risks and provided practical implications for the precise mitigation of targeted sources

and components to alleviate the human health risks posed by $PM_{2.5}$ pollution, taking site-specific scenarios into consideration. Our study along with others' highlighted the need to consider the health protection goal-based source apportionment and emission mitigation in supplement to the current mass concentration-based framework. As such, future studies are warranted to resolve the contribution of driving components and their sources to $PM_{2.5}$ toxicities and/or health risks.

Declaration of interest

The authors declare that they have no competing financial interests.

Acknowledgments

This study was supported by the National Natural Science Foundation of China (NSFC 91543205), the National Key R&D Program of China (2017YFC0212000), and the Research Grants Council of Hong Kong (PolyU 152095/14E and 152106/18E). The XANES spectra were acquired on beamline 01C1 in the NSRRC, Taiwan. We thank Dr. Ting-shan Chan from the NSRRC for his kind help in collecting the spectral data, Dr. Yanping Zhao from the Guangdong Institute of Analysis for her kind instruction on the spectral interpretation of arsenic speciation, and Jie Ding from the National Center for Nanoscience and Technology and Liyan Tian from Nanjing University for their help with the analysis of OC and EC.

References

Atkinson, R., Kang, S., Anderson, H., Mills, I., Walton, H., 2014. Epidemiological time series studies of $PM_{2.5}$ and daily mortality and hospital admissions: a systematic review and meta-analysis. Thorax, 69, 660-665.

Chan, L. Y., Chu, K. W., Zou, S. C., Chan, C. Y., Wang, X. M., Barletta, B., Blake, D. R., Hui, G., Tsai, W. Y., 2006. Characteristics of nonmethane hydrocarbons (NMHCs) in industrial, industrial-urban, and industrial-suburban atmospheres of the Pearl River Delta (PRD) region of south China. J. Geophys. Res.: Atmos., 111, doi:10.1029/2005JD006481.

Chang, Y., Huang, K., Deng, C., Zou, Z., Liu, S., Zhang, Y., 2017. First long-term and near real-time measurement of atmospheric trace elements in Shanghai, China. Atmos. Chem. Phys., 18, 11793-11812.

Cong, Z., Kang, S., Luo, C., Li, Q., Huang, J., Gao, S., Li, X., 2011. Trace elements and lead isotopic composition of PM_{10} in Lhasa, Tibet. Atmos. Environ., 45, 6210-6215.

Cui, J., Du, J., Tian, H., Chan, T., Jing, C., 2018. Rethinking anaerobic As (III) oxidation in filters: Effect of indigenous nitrate respirers. Chemosphere, 196, 223-230.

Cui, J., Shi, J., Jiang, G., Jing, C., 2013. Arsenic levels and speciation from ingestion exposures to biomarkers in Shanxi, China: implications for human health. Environ. Sci. Technol., 47, 5419-5424.

Du, W., Zhang, Y., Chen, Y., Xu, L., Chen, J., Deng, J., Hong, Y., Xiao, H., 2017. Chemical characterization and source apportionment of $PM_{2.5}$ during spring and winter in the Yangtze River Delta, China. Aerosol Air Qual. Res., 17, 2165-2180.

Egorova, K. S., Ananikov, V. P., 2017. Toxicity of metal compounds: knowledge and myths. Organometallics, 36, 4071-4090.

Guangdong Geological Survey, 2010. Multi-purposes geochemical survey: Pearl River Delta, Guangdong province.

Huang, M., Chen, X., Zhao, Y., Chan, C. Y., Wang, W., Wang, X., Wong, M. H., 2014. Arsenic speciation in total contents and bioaccessible fractions in atmospheric particles related to human intakes. Environ. Pollut., 188, 37-44.

Huang, R., Cheng, R., Jing, M., Yang, L., Li, Y., Chen, Q., Chen, Y., Yan, J., Lin, C., Wu, Y., 2018. Source-specific health risk analysis on particulate trace elements: Coal combustion and traffic emission as major contributors in wintertime Beijing. Environ. Sci. Technol., 52, 10967-10974.

Huang, X., Betha, R., Tan, L., Balasubramanian, R., 2016a. Risk assessment of

548 bioaccessible trace elements in smoke haze aerosols versus urban aerosols using
549 simulated lung fluids. Atmos. Environ., 125, 505-511.
550
551 Huang, X., Cheng, J., Bo, D., Betha, R., Balasubramanian, R., 2016b. Bioaccessibility
552 of Airborne Particulate-Bound Trace Elements in Shanghai and Health Risk
553 Assessment. Front. Environ. Sci., 4, 76.
554
555 Hueglin, C., Gehrig, R., Baltensperger, U., Gysel, M., Monn, C., Vonmont, H., 2005.
556 Chemical characterisation of $PM_{2.5}$, PM_{10} and coarse particles at urban, near-city and
557 rural sites in Switzerland. Atmos. Environ., 39, 637-651.
558
559 Jan, A., Azam, M., Siddiqui, K., Ali, A., Choi, I., Haq, Q., 2015. Heavy metals and
560 human health: mechanistic insight into toxicity and counter defense system of
561 antioxidants. Int. J. Mol. Sci., 16, 29592-29630.
562
563 Jin, L., Luo, X. S., Fu, P. Q., Li, X.D., 2017. Airborne particulate matter pollution in
564 urban China: A chemical mixture perspective from sources to impacts. Natl. Sci. Rev.,
565 4, 593-610.
566
567 Jin, L., Xie, J. W., Wong, C. K.-C., Chan, S. K., Abbaszade, G., Schnelle-Kreis, J.,
568 Zimmermann, R., Li, J., Zhang, G., Fu, P. Q., Li, X. D. 2019. Contributions of city-
569 specific $PM_{2.5}$ to differential in vitro oxidative stress and toxicity implications between
570 Beijing and Guangzhou of China. Environ. Sci. Technol., 53, 2881-2891.
571
572 Kendall, M., Pala, K., Ucakli, S., Gucer, S., 2011. Airborne particulate matter ($PM_{2.5}$
573 and PM_{10}) and associated metals in urban Turkey. Air Qual., Atmos. Health, 4, 235-242.
574
575 Labrada-Delgado, G., Aragon-Pina, A., Campos-Ramos, A., Castro-Romero, T.,
576 Amador-Munoz, O., Villalobos-Pietrini, R., 2012. Chemical and morphological
577 characterization of $PM_{2.5}$ collected during MILAGRO campaign using scanning
578 electron microscopy. Atmos. Pollut. Res., 3, 289-300.
579
580 Li, X. D., Jin, L., Kan, H. D., 2019a. Air pollution: a global problem needs local fixes.
581 Nature, 570, 437-439.
582
583 Li, Y., Juhasz, A. L., Ma, L. Q., Cui, X., 2019b. Inhalation bioaccessibility of PAHs in
584 $PM_{2.5}$: Implications for risk assessment and toxicity prediction. Sci. Total Environ., 650,
585 56-64.
586
587 Liao, Q., Liu, C., Jin, Y., Hua, M., Zheng, L., Pan, Y., Huang, S., 2011. On geochemical
588 regionalization of soils in Jiangsu (in Chinese). J. Geol., 35, 225-235.
589
590 Liu, P., Lei, Y., Ren, H., Gao, J., Xu, H., Shen, Z., Zhang, Q., Zheng, C., Liu, H., Zhang,
591 R., 2017. Seasonal Variation and Health Risk Assessment of Heavy Metals in $PM_{2.5}$

during Winter and Summer over Xi'an, China. Atmosphere, 8, 91.

Lu, S., Yao, Z., Chen, X., Wu, M., Sheng, G., Fu, J., Daly, P., 2008. The relationship between physicochemical characterization and the potential toxicity of fine particulates ($PM_{2.5}$) in Shanghai atmosphere. Atmos. Environ., 42, 7205-7214.

Mahapatra, P. S., Jain, S., Shrestha, S., Senapati, S., Puppala, S. P., 2018. Ambient endotoxin in PM_{10} and association with inflammatory activity, air pollutants, and meteorology, in Chitwan, Nepal. Sci. Total Environ., 618, 1331-1342.

Malm, W. C., Schichtel, B. A., Hand, J. L., Collett, J. L., 2017. Concurrent Temporal and Spatial Trends in Sulfate and Organic Mass Concentrations Measured in the IMPROVE Monitoring Program. J. Geophys. Res.: Atmos., 122, 10,462-410,476.

Ming, L.L, Jin, L., Li, J., Fu, P.Q., Yang, W.Y., Liu, D., Zhang, G., Wang, Z.F., Li, X.D., 2017. $PM_{2.5}$ in the Yangtze River Delta, China: Chemical compositions, seasonal variations, and regional pollution events. Environ. Pollut., 223, 200-212.

National Bureau of Statistics of China, 2014. China Energy Statistical Yearbook 2014.

Norris, G. A., Duvall, R., Brown, S. G., Bai, S., 2014. EPA Positive Matrix Factorization (PMF) 5.0 Fundamentals and User Guide. U.S. Environmental Protection Agency, Washington, DC, EPA/600/R-14/108 (NTIS PB2015-105147).

OEHHA, 2014. Inorganic arsenic reference exposure levels Sacramento, CA Office of Environmental Health Hazard Assessment; California EPA HERO ID 3484946.

Oosthuizen, M. A., Wright, C. Y., Matooane, M., Phala, N., 2015. Human health risk assessment of airborne metals to a potentially exposed community: a screening exercise. Clean Air J., 25, DOI:10.17159/12410-17972X/12015/v17125n17151a17155.

Qi, L., Chen, M., Ge, X., Zhang, Y., Guo, B., 2016. Seasonal variations and sources of 17 aerosol metal elements in suburban Nanjing, China. Atmosphere, 7, 153.

Ravel, B., Newville, M., 2005. ATHENA, ARTEMIS, HEPHAESTUS: data analysis for X-ray absorption spectroscopy using IFEFFIT. J. Synchrotron Radiat., 12, 537-541.

Sánchez-Rodas, D., de la Campa, A. M. S., Jesús, D., Oliveira, V., Gómez-Ariza, J. L., Querol, X., Alastuey, A., 2007. Arsenic speciation of atmospheric particulate matter (PM10) in an industrialised urban site in southwestern Spain. Chemosphere, 66, 1485-1493.

Smichowski, P., Polla, G., Gómez, D., 2005. Metal fractionation of atmospheric aerosols via sequential chemical extraction: a review. Anal. Bioanal. Chem., 381, 302-

316.

Sørensen, M., Schins, R. P., Hertel, O., Loft, S., 2005. Transition metals in personal samples of $PM_{2.5}$ and oxidative stress in human volunteers. Cancer Epidemiol. Biomarkers Prev., 14, 1340-1343.

Taghvaee, S., Sowlat, M. H., Hassanvand, M. S., Yunesian, M., Naddafi, K., Sioutas, C., 2018. Source-specific lung cancer risk assessment of ambient $PM_{2.5}$-bound polycyclic aromatic hydrocarbons (PAHs) in central Tehran. Environ. Int., 120, 321-332.

Tan, J., Duan, J., Ma, Y., Yang, F., Cheng, Y., He, K., Yu, Y., Wang, J., 2014. Source of atmospheric heavy metals in winter in Foshan, China. Sci. Total Environ., 493, 262-270.

Tao, J., Zhang, L., Cao, J., Zhong, L., Chen, D., Yang, Y., Chen, D., Chen, L., Zhang, Z., Wu, Y., 2017. Source apportionment of $PM_{2.5}$ at urban and suburban areas of the Pearl River Delta region, south China-with emphasis on ship emissions. Sci. Total Environ., 574, 1559-1570.

Thurston, G. D., Burnett, R. T., Turner, M. C., Shi, Y., Krewski, D., Lall, R., Ito, K., Jerrett, M., Gapstur, S. M., Diver, W. R., 2016. Ischemic heart disease mortality and long-term exposure to source-related components of US fine particle air pollution. Environ. Health Perspect., 124, 785–794.

USEPA, 2007. Arsenic, inorganic (CASRN 7440-38-2).

USEPA, 2018. Regional Screening Levels (RSLs) - Generic Tables (2018), US Environmental Protection Agency Washington, DC. Available at https://www.epa.gov/risk/regional-screening-levels-rsls-generic-tables.

Wang, X., He, S., Chen, S., Zhang, Y., Wang, A. h., Luo, J., Ye, X., Mo, Z., Wu, L., Xu, P., 2018. Spatiotemporal characteristics and health risk assessment of heavy metals in $PM_{2.5}$ in Zhejiang Province. Int. J. Environ. Res. Public Health, 15, 583.

Wang, Y. H., Hu, L. F., Lu, G. H., 2015. Health risk assessments based on existing data of arsenic, chromium, lead, and zinc in China's air. Hum. Ecol. Risk Assess., 21, 560-573.

WHO, 2018. Ambient (outdoor) air quality and health. Available: https://www.who.int/news-room/fact-sheets/detail/ambient-(outdoor)-air-quality-and-health.

Wiseman, C. L., Zereini, F., 2014. Characterizing metal (loid) solubility in airborne

PM_{10}, $PM_{2.5}$ and PM_1 in Frankfurt, Germany using simulated lung fluids. Atmos. Environ., 89, 282-289.

Yang, G., Ma, L., Xu, D., Li, J., He, T., Liu, L., Jia, H., Zhang, Y., Chen, Y., Chai, Z., 2012. Levels and speciation of arsenic in the atmosphere in Beijing, China. Chemosphere, 87, 845-850.

Zereini, F., Wiseman, C. L., Püttmann, W., 2012. In vitro investigations of platinum, palladium, and rhodium mobility in urban airborne particulate matter (PM_{10}, $PM_{2.5}$, and PM_1) using simulated lung fluids. Environ. Sci. Technol., 46, 10326-10333.

Zhou, S., Davy, P. K., Huang, M., Duan, J., Wang, X., Fan, Q., Chang, M., Liu, Y., Chen, W., Xie, S., 2018. High-resolution sampling and analysis of ambient particulate matter in the Pearl River Delta region of southern China: source apportionment and health risk implications. Atmos. Chem. Phys., 18, 2049-2064.

Zhuo, S., Shen, G., Zhu, Y., Du, W., Pan, X., Li, T., Han, Y., Li, B., Liu, J., Cheng, H., 2017. Source-oriented risk assessment of inhalation exposure to ambient polycyclic aromatic hydrocarbons and contributions of non-priority isomers in urban Nanjing, a megacity located in Yangtze River Delta, China. Environ. Pollut., 224, 796-809.

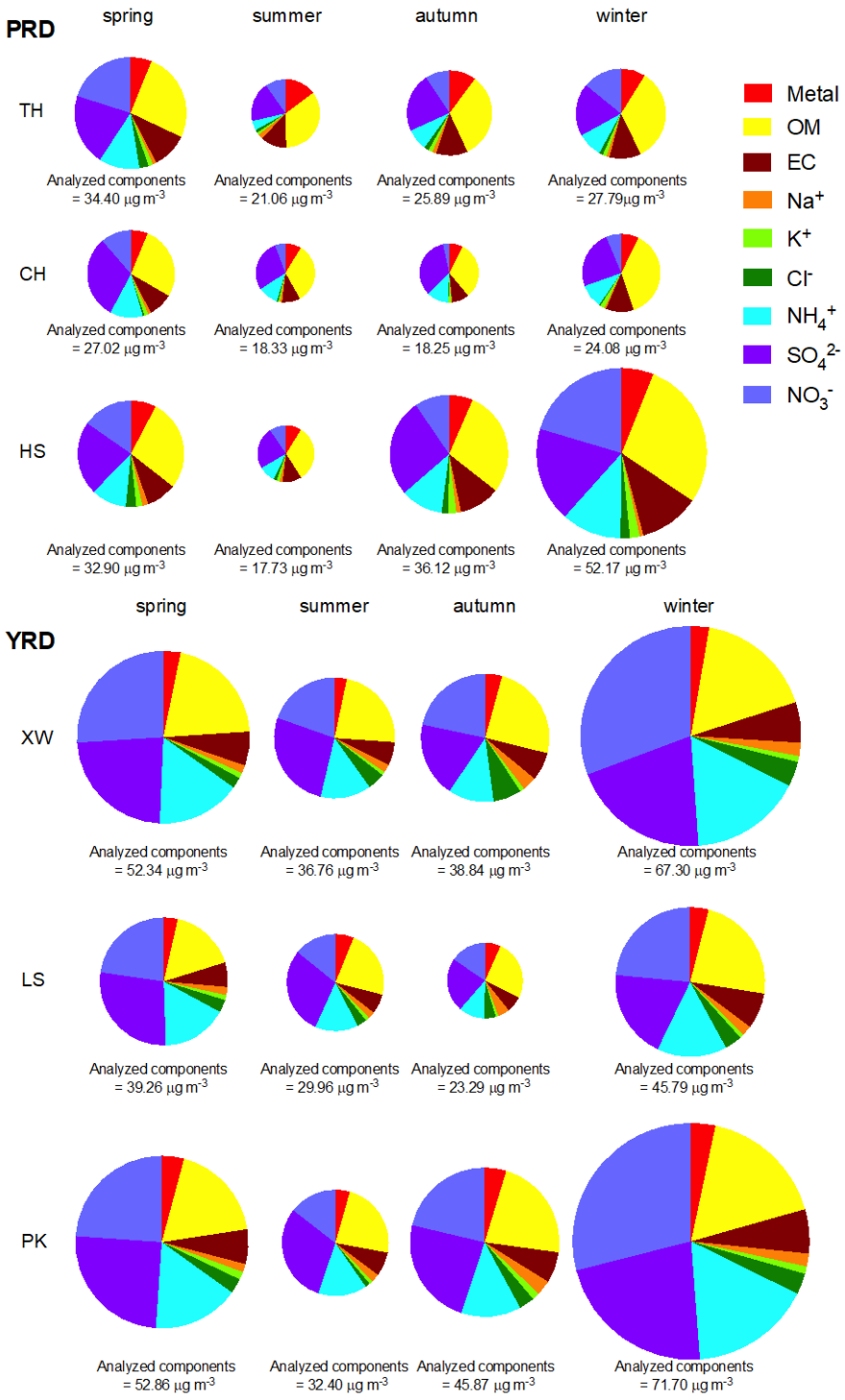

Figure 1. Seasonal variations in major chemical components analyzed in $PM_{2.5}$ in the PRD and YRD regions. The pies are divided according to the proportion that each analyzed component contributes to total concentration of $PM_{2.5}$ in the sample. Organic

706 matter (OM) was estimated by multiplying the organic carbon content by a factor of
707 1.8 (Malm et al., 2017).

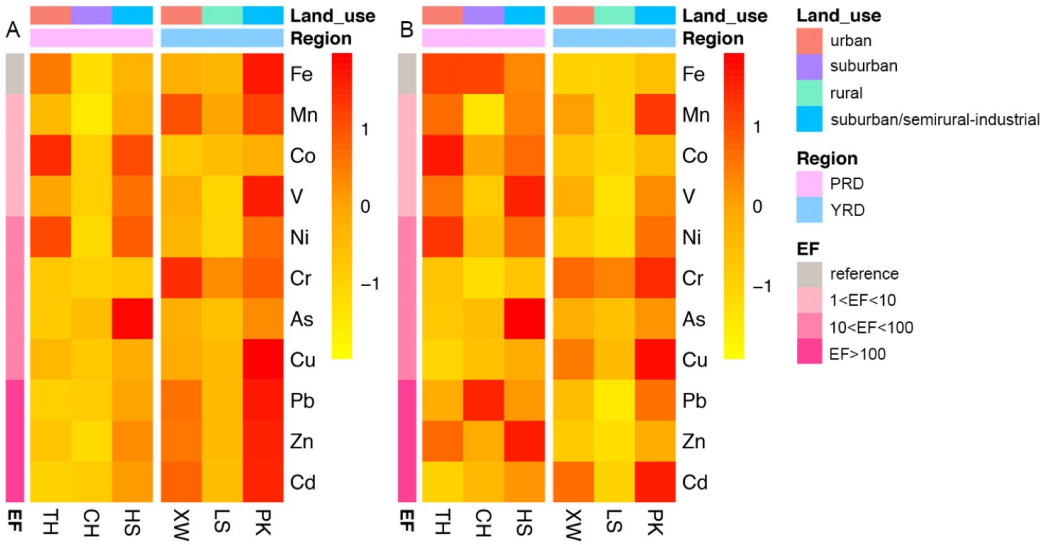

Figure 2. Comparisons of total (A) and bioaccessible (B) metal/metalloid concentrations in $PM_{2.5}$ in the PRD and YRD regions based on annual average figures. The concentration value of each element was normalized independently prior to plotting figures in R using a package pheatmap. The original data is found in the supplemental material (Table S9, Table S10). Metals presented here were grouped based on the mean value of the enrichment factors in all the sampling sites.

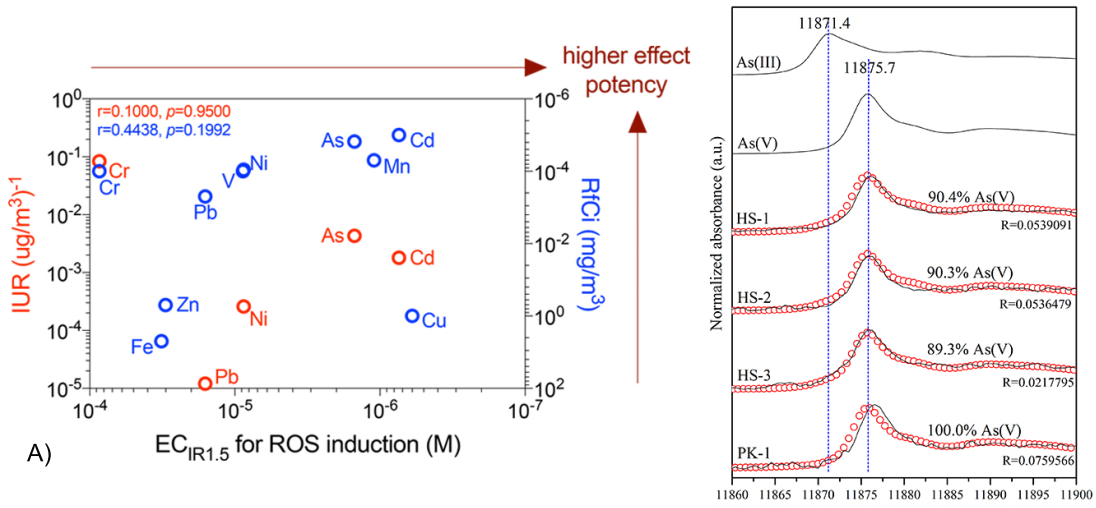

715

716 **Figure 3.** Toxicity potency of metal with regard to its speciation. Subfigure A) shows
717 the correlation (spearman r and *p* values are shown) between the effect concentration
718 ($EC_{IR1.5}$) for the reactive oxygen species (ROS) induction (M) of different metals
719 revealed in our previous study (Jin et al., 2019) and the inhalation unit risk $(\mu g/m^3)^{-1}$
720 (IUR), as well as the reference concentration (mg/m^3) via inhalation (RfC_i) of various
721 metals specified in the documents of the USEPA (2018) and other national standards
722 (Oosthuizen et al., 2015) that are given in Table S7. The $EC_{IR1.5}$ data of the different
723 metals used here are based on certain kinds of speciation, *i.e.*, Pb(II), V(V), Ni(II),
724 As(V), Mn(II), Cr(III), Cd(II), Fe(III), Cu(II), and Zn(II). Subfigure B) presents the
725 dominant speciation of arsenic in three $PM_{2.5}$ samples with high concentrations of
726 arsenic in the semirural-industrial site (HS) in the PRD and one in the suburban-
727 industrial site (PK) in the YRD, illustrated by X-ray absorption near the edge structure
728 (XANES) spectra (black solid line). The red dotted lines represented the LCF results.
729 The spectra of two standards (As(III) and As(V)) were obtained from a previous study
730 (Cui et al., 2013).

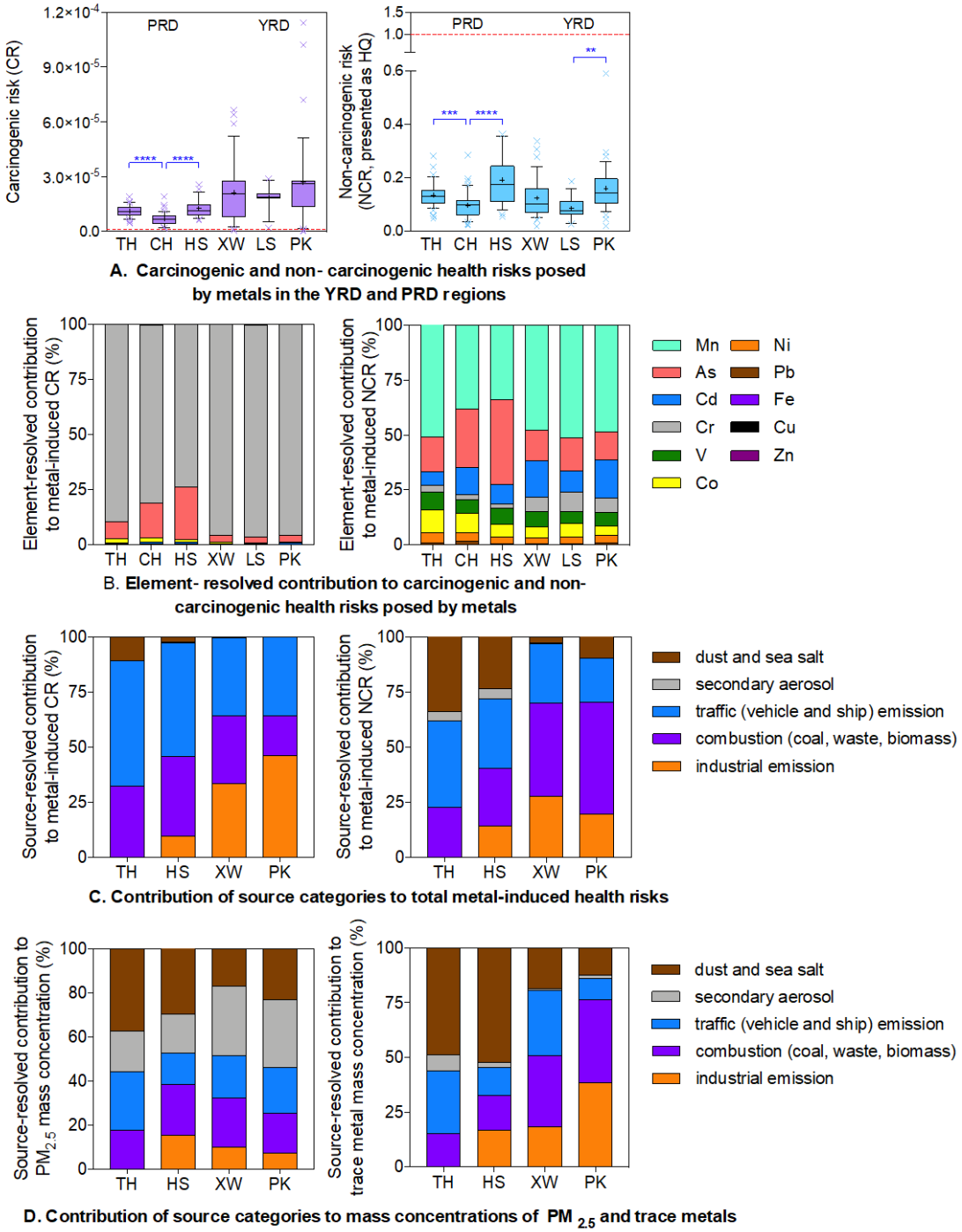

Figure 4. Risk-oriented source apportionment of $PM_{2.5}$-associated metals in the PRD and YRD regions. Panel A presents carcinogenic risks and non-carcinogenic risks posed by metals across land-use gradients in the two studied regions based on annual average bioaccessible metal concentrations, with modifications according to As

speciation. The box plots with whiskers cover data from the 10^{th} to 90^{th} percentiles, with outliers marked by crosses. The red dashed lines stand for the acceptable risk levels for carcinogens (10^{-6}) and the reference level of hazard quotients (1.0) for non-cancer effects recommended by the USEPA. Panel B indicates the relative contributions of various metals to the total carcinogenic and non-carcinogenic risks in the six sampling sites. Panel C points out the urban-industrial contrast in source-specific health risks posed by trace metals in the PRD and the YRD regions. Panel D supplements the source-resolved mass profiles of $PM_{2.5}$ and risk-inducing trace metals (Mn, As, Cd, Cr, V, Co, Ni, Pb, Fe, Cu, and Zn).